INTERNATIONAL JOURNAL FOR NUMERICAL METHODS IN FLUIDS, VOL. 13, 1289–1310 (1991)

A FINITE DIFFERENCE ANALYSIS OF THE EXTRUDATE SWELL PROBLEM

YOUNG-CHEOL AHN AND MICHAEL E. RYAN*

Department of Chemical Engineering, State University of New York at Buffalo, Buffalo, NY 14260, U.S.A.

SUMMARY

The extrudate swell phenomenon of a purely viscous fluid is analysed by solving simultaneously the Cauchy momentum equations along with the continuity equation by means of a finite difference method. The circular and planar jet flows of Newtonian and power-law fluids are simulated using a control volume finite difference method suggested by Patankar called SIMPLER (semi-implicit method for pressure-linked equations). This method uses the velocity components and pressure as the primitive variables and employs a staggered grid and control volume for each separate variable. The numerical results show good agreement with the analytical solution of the axisymmetric stick–slip problem and exhibit a Newtonian swelling ratio of 13.2% or 19.2% for a capillary or slit die respectively in accordance with previously reported experimental and numerical results. Shear thinning results in a decrease in swelling ratio, as does the introduction of gravity and surface tension.

KEY WORDS Extrudate swell Jet swell Stick–slip problem Control volume Finite difference method

INTRODUCTION

The flow of highly viscous fluids such as polymer melts is commonly encountered in the materials-processing industry and many applications are conducted in the low-Reynolds-number regime. Such applications include pipe and profile extrusion which is used in the production of rods, pipes, sheets and a wide variety of other final products. The extrusion process is not only of technological interest but also constitutes a challenging problem for numerical simulation owing to the presence of mixed boundary conditions and a stress singularity at the die exit. Once the fluid emerges from the die, it exhibits the characteristic phenomenon known as 'extrudate swell' or 'jet swell'. Extrudate swell is most commonly given as the ratio of the extrudate dimension to the die dimension or as the change of extrudate dimension in reference to the die dimension expressed as a percentage. These definitions provide a quantitative measure of the swelling behaviour. The jet swell ratio is strongly dependent on the rheological properties of the liquid as well as other factors. Experimentally, the jet swell ratio has been found to be approximately 1.1–1.2 for Newtonian fluids[1–5] and to typically range from two to three for viscoelastic liquids.[6–8]

Theoretical analysis of the jet swell phenomenon has been attempted both analytically and numerically. Analytical approaches have been successfully applied to the stick–slip problem.[9–11]

* Author to whom correspondence should be addressed.

0271–2091/91/201289–22$11.00

Received 26 May 1990
Revised 3 April 1991

However, analytical investigation of the swelling phenomenon has rarely been reported[12] and will continue to remain a formidable challenge for the foreseeable future.

Over the past 15 years numerous numerical studies of the jet swell problem have been undertaken and considerable progress has been realized with the steady improvement in computational hardware as well as software codes. Most of these numerical studies have employed finite element methods. Since the first successful numerical analysis of the creeping flow of a Newtonian jet by Nickell *et al.*,[4] several other analyses of the problem have been published.[13-22] The creeping jet flow of a viscoelastic fluid has even been successfully analysed using finite element methods for fluids exhibiting weakly elastic behaviour.[23-28]

Reddy and Tanner[23] used a second-order fluid model in order to predict the swelling of a plane jet, whereas Chang *et al.*[24] employed a non-linear Maxwell model for both axisymmetric and planar geometries. Tuna and Finlayson[28] obtained convergence for the jet swell of a convected Maxwell fluid up to Wissenberg numbers of 1·6 for cylindrical geometry and 1·05 for planar geometry using a Galerkin finite element method. Crochet and Keunings[25] reported calculations for the jet swell of a convected Maxwell fluid using a mixed finite element method. These authors also reported successful calculations for an Oldroyd B fluid model exhibiting high elastic behaviour with recoverable shear values as large as four.[26] In order to achieve higher Weissenberg numbers, some authors such as Wesson and Papanastasiou[29] and Phan-Thien[30] employed a slip boundary condition at the wall. Marchal and Crochet[31] employed a mixed finite element technique to successfully calculate the flow of Maxwell B and Oldroyd B fluids at very high values of Deborah number.

On the other hand, very few numerical studies of the jet swell phenomenon have employed finite difference methods. A tranditional finite difference method was first employed by Horsfall[32] to analyse the Newtonian jet swell phenomenon. His numerical solution, however, predicted a swelling ratio considerably smaller than that observed experimentally, owing to inaccuracies of interpolation in enforcing the boundary conditions at the free surface. The only finite difference technique which successfully predicted the jet swell phenomenon was undertaken by Dutta and Ryan[33] for the creeping Newtonian jet flow through axisymmetric and slit dies. They employed a streamfunction–vorticity formulation to eliminate the need for satisfying mass continuity and adopted an orthogonal curvilinear co-ordinate system to accommodate the irregular boundary.

In the present method a finite difference formulation using a staggered grid and control volume approach, with velocity and pressure as the primitive variables, is employed. The irregular shape of the physical domain is transformed into a rectangular computational domain in order to facilitate discretization without difficulties arising from the changing shape of the free boundary. The predicted creeping jet swell of Newtonian and power-law fluids is discussed along with the details of the present technique.

A schematic diagram of the extrudate swell problem is presented in Figure 1 along with the prescribed boundary conditions. The fluid comes in as a fully developed flow at the far upstream boundary, passes through the die exit and ultimately moves without any stresses far downstream. On the die wall the no-slip condition is applied, while on the free surface the tangential stress is equal to zero, the normal stress is balanced by surface tension and the no-penetration condition is applied. At the centreline a symmetry condition is applied.

FORMULATION

The governing equations that describe the motion of a fluid jet are the momentum equations and the continuity equation. The following assumptions are employed for this flow problem: (a) steady state, (b) incompressible, (c) two-dimensional or axisymmetric. The continuity and

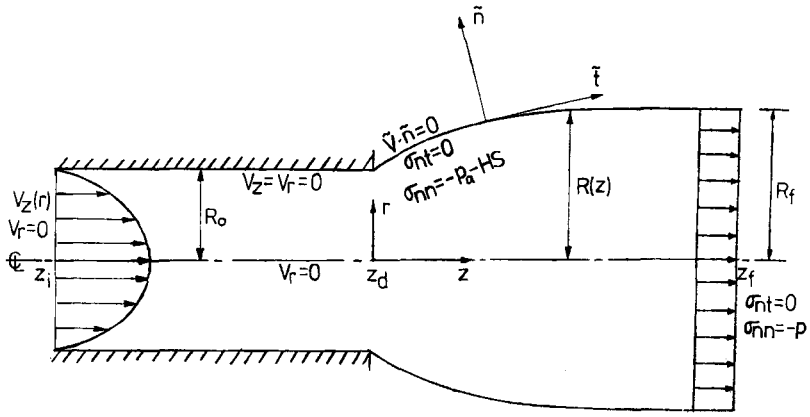

Figure 1. Schematic diagram of jet swell problem with prescribed boundary conditions

Cauchy momentum equations in normalized form are

$$\frac{1}{r^\alpha}\frac{\partial}{\partial r}(r^\alpha v_r)+\frac{\partial v_z}{\partial z}=0, \tag{1}$$

$$Re\left(v_r\frac{\partial v_r}{\partial r}+v_z\frac{\partial v_r}{\partial z}\right)=-\frac{\partial p}{\partial r}+\frac{\partial \tau_{rr}}{\partial r}+\alpha\frac{\tau_{rr}-\tau_{\theta\theta}}{r}+\frac{\partial \tau_{rz}}{\partial z}+G_r, \tag{2}$$

$$Re\left(v_r\frac{\partial v_z}{\partial r}+v_z\frac{\partial v_z}{\partial z}\right)=-\frac{\partial p}{\partial z}+\frac{\partial \tau_{rz}}{\partial r}+\alpha\frac{\tau_{rz}}{r}+\frac{\partial \tau_{zz}}{\partial z}+G_z. \tag{3}$$

The equations have been normalized using a characteristic length L (defined as the half-channel width or die radius), a characteristic velocity V (defined as the average flow velocity) and a characteristic viscosity $K(V/L)^{n-1}$, where K and n are the consistency index and power-law index respectively. The Reynolds number and body forces are denoted as $Re=\rho L^n V^{2-n}/K$ and $G_i=\rho L^{n+1}g_i/KV^n$ respectively. The pressure and stress terms are normalized by KV^n/L^n. The parameter α determines the co-ordinate system for the geometry of interest, i.e. $\alpha=0$ for rectangular co-ordinates associated with slit dies and $\alpha=1$ for cylindrical co-ordinates associated with capillary dies. For the creeping flow of a highly viscous liquid, $Re\ll 1$ and the inertial terms in the momentum equation can be ignored. For this situation the creeping flow equations are

$$0=-\frac{\partial p}{\partial r}+\frac{\partial \tau_{rr}}{\partial r}+\alpha\frac{\tau_{rr}-\tau_{\theta\theta}}{r}+\frac{\partial \tau_{rz}}{\partial z}+G_r, \tag{4}$$

$$0=-\frac{\partial p}{\partial z}+\frac{\partial \tau_{rz}}{\partial r}+\alpha\frac{\tau_{rz}}{r}+\frac{\partial \tau_{zz}}{\partial z}+G_z. \tag{5}$$

For the generalized Newtonian fluid the constitutive equation yields

$$\tau_{rr}=2\mu\frac{\partial v_r}{\partial r},\qquad \tau_{\theta\theta}=2\mu\frac{v_r}{r},\qquad \tau_{zz}=2\mu\frac{\partial v_z}{\partial z},\qquad \tau_{rz}=\mu\left(\frac{\partial v_r}{\partial z}+\frac{\partial v_z}{\partial r}\right). \tag{6}$$

For a power-law fluid the viscosity is related to the second scalar invariant of the rate-of-deformation tensor as follows:

$$\mu=|\tfrac{1}{2}\Pi|^{(n-1)/2}, \tag{7}$$

where

$$\tfrac{1}{2}\Pi = 2\left[\left(\frac{\partial v_r}{\partial r}\right)^2 + \alpha\left(\frac{v_r}{r}\right)^2 + \left(\frac{\partial v_z}{\partial z}\right)^2\right] + \left(\frac{\partial v_r}{\partial z} + \frac{\partial v_z}{\partial r}\right)^2. \tag{8}$$

Substituting the constitutive equation into the momentum equation and rearranging gives

$$0 = -r^\alpha \frac{\partial p}{\partial r} + \frac{\partial}{\partial r}\left(\mu r^\alpha \frac{\partial v_r}{\partial r}\right) + \frac{\partial}{\partial z}\left(\mu r^\alpha \frac{\partial v_r}{\partial z}\right) - \alpha\mu \frac{v_r}{r} + r^\alpha\left(\frac{\partial \mu}{\partial r}\frac{\partial v_r}{\partial r} + \frac{\partial \mu}{\partial z}\frac{\partial v_z}{\partial r}\right), \tag{9}$$

$$0 = -r^\alpha \frac{\partial p}{\partial z} + \frac{\partial}{\partial r}\left(\mu r^\alpha \frac{\partial v_z}{\partial r}\right) + \frac{\partial}{\partial z}\left(\mu r^\alpha \frac{\partial v_z}{\partial z}\right) + r^\alpha\left(\frac{\partial \mu}{\partial r}\frac{\partial v_r}{\partial z} + \frac{\partial \mu}{\partial z}\frac{\partial v_z}{\partial z} + G_z\right), \tag{10}$$

where the body forces in the radial direction have been neglected.

The above equations are formulated in the physical domain together with the following boundary conditions:

(i) $z = z_i,\ 0 \leqslant r \leqslant 1$: $\quad v_z = v_z(r) = \dfrac{(\alpha+2)n+1}{n+1}(1 - r^{(n+1)/n}),\quad v_r = 0;$

(ii) $z_i \leqslant z \leqslant z_f,\ r = 0$: $\quad v_r = 0,\quad (\boldsymbol{\sigma}\cdot\mathbf{n})\cdot\mathbf{t} = 0;$

(iii) $z = z_f,\ 0 \leqslant r \leqslant R_f$: $\quad (\boldsymbol{\sigma}\cdot\mathbf{n})\cdot\mathbf{t} = 0,\quad (\boldsymbol{\sigma}\cdot\mathbf{n})\cdot\mathbf{n} = -p;$

(iv) $z_i \leqslant z \leqslant z_d,\ r = 1$: $\quad v_z = 0,\quad v_r = 0;$

(v) $z_d \leqslant z \leqslant z_f,\ r = R(z)$: $\quad (\boldsymbol{\sigma}\cdot\mathbf{n})\cdot\mathbf{t} = 0,\quad (\boldsymbol{\sigma}\cdot\mathbf{n})\cdot\mathbf{n} = -p_a - HS,\quad \mathbf{v}\cdot\mathbf{n} = 0.$ (11)

Here z_i and z_f denote the axial co-ordinates of the upstream and downstream boundaries respectively and z_d is the axial co-ordinate associated with the die exit. $R(z)$ is the location of the free surface as a function of axial distance z, $S = \sigma L^{n-1}/KV^n$ is the surface tension parameter and H is the total curvature of the free surface defined by

$$H = \frac{-\mathrm{d}^2 R/\mathrm{d}z^2}{[1 + (\mathrm{d}R/\mathrm{d}z)^2]^{3/2}} + \frac{\alpha}{R[1 + (\mathrm{d}R/\mathrm{d}z)^2]^{1/2}}. \tag{12}$$

Condition (i) corresponds to fully developed flow in the upstream region, (ii) is the symmetry condition at the centreline, (iii) is the condition of zero deviatoric stresses far downstream, (iv) is the no-slip condition at the wall and (v) is the condition on the free surface characterized by zero shear stress, normal force balance and no penetration.

In order to facilitate the numerical analysis, the physical co-ordinates z and r are transformed into the computational co-ordinates ζ and η by means of the relationships

$$\zeta = z, \qquad \eta = \frac{r}{R(z)}, \qquad \frac{\partial}{\partial z} = \frac{\partial}{\partial \zeta} - \frac{\eta}{R}\frac{\mathrm{d}R}{\mathrm{d}\zeta}\frac{\partial}{\partial \eta}, \qquad \frac{\partial}{\partial r} = \frac{1}{R}\frac{\partial}{\partial \eta}. \tag{13}$$

This co-ordinate-stretching method is similar to the approach used for the orthogonal collocation method in Reference 24. The continuity and momentum equations may be transformed to the following expressions in the computational domain

$$\frac{\partial}{\partial \eta}\left((\eta R)^\alpha v_r - (\eta R)^\alpha \eta \frac{\mathrm{d}R}{\mathrm{d}\zeta} v_z\right) + \frac{\partial}{\partial \zeta}[(\eta R)^\alpha R v_z] = 0, \tag{14}$$

$$0 = \frac{\partial}{\partial \eta}\left(C_\eta \frac{\partial v_r}{\partial \eta}\right) + \frac{\partial}{\partial \zeta}\left(C_\zeta \frac{\partial v_r}{\partial \zeta}\right) - P_\eta + S_\eta, \tag{15}$$

$$0 = \frac{\partial}{\partial \eta}\left(C_\eta \frac{\partial v_z}{\partial \eta}\right) + \frac{\partial}{\partial \zeta}\left(C_\zeta \frac{\partial v_z}{\partial \zeta}\right) - P_\zeta + S_\zeta, \tag{16}$$

where

$$C_\eta=\frac{\mu}{R^2}(\eta R)^\alpha, \qquad C_\zeta=\mu(\eta R)^\alpha, \qquad P_\eta=\frac{(\eta R)^\alpha}{R}\frac{\partial p}{\partial \eta}, \qquad P_\zeta=(\eta R)^\alpha\frac{\partial p}{\partial \zeta},$$

$$\begin{aligned}S_\eta=(\eta R)^\alpha\Bigg[&-\frac{\eta}{R}\frac{\mathrm{d}R}{\mathrm{d}\zeta}\frac{\partial\mu}{\partial\zeta}\frac{\partial v_r}{\partial\eta}+2\frac{\mu\eta}{R^2}\left(\frac{\mathrm{d}R}{\mathrm{d}\zeta}\right)^2\frac{\partial v_r}{\partial\eta}-\frac{\mu\eta}{R}\frac{\mathrm{d}^2R}{\mathrm{d}\zeta^2}\frac{\partial v_r}{\partial\eta}-2\frac{\mu\eta}{R}\frac{\mathrm{d}R}{\mathrm{d}\zeta}\frac{\partial^2 v_r}{\partial\zeta\,\partial\eta}\\&-\frac{\eta}{R}\frac{\mathrm{d}R}{\mathrm{d}\zeta}\frac{\partial\mu}{\partial\eta}\frac{\partial v_r}{\partial\zeta}-\alpha\frac{\mu}{R}\frac{\mathrm{d}R}{\mathrm{d}\zeta}\frac{\partial v_r}{\partial\zeta}+\left(\frac{\eta}{R}\frac{\mathrm{d}R}{\mathrm{d}\zeta}\right)^2\frac{\partial\mu}{\partial\eta}\frac{\partial v_r}{\partial\eta}+\mu\left(\frac{\eta}{R}\frac{\mathrm{d}R}{\mathrm{d}\zeta}\right)^2\frac{\partial^2 v_r}{\partial\eta^2}\\&-\alpha\frac{\mu v_r}{(\eta R)^{\alpha+1}}+\frac{1}{R^2}\frac{\partial\mu}{\partial\eta}\frac{\partial v_r}{\partial\eta}+\frac{1}{R}\frac{\partial\mu}{\partial\zeta}\frac{\partial v_z}{\partial\eta}-\frac{\eta}{R^2}\frac{\mathrm{d}R}{\mathrm{d}\zeta}\frac{\partial\mu}{\partial\eta}\frac{\partial v_z}{\partial\eta}\Bigg],\end{aligned} \tag{17}$$

$$\begin{aligned}S_\zeta=(\eta R)^\alpha\Bigg[&\frac{\eta}{R}\frac{\mathrm{d}R}{\mathrm{d}\zeta}\frac{\partial p}{\partial\eta}-2\frac{\eta}{R}\frac{\mathrm{d}R}{\mathrm{d}\zeta}\frac{\partial\mu}{\partial\zeta}\frac{\partial v_z}{\partial\eta}+2\frac{\mu\eta}{R^2}\left(\frac{\mathrm{d}R}{\mathrm{d}\zeta}\right)^2\frac{\partial v_z}{\partial\eta}-\frac{\mu\eta}{R}\frac{\mathrm{d}^2R}{\mathrm{d}\zeta^2}\frac{\partial v_z}{\partial\eta}\\&-2\frac{\mu\eta}{R}\frac{\mathrm{d}R}{\mathrm{d}\zeta}\frac{\partial^2 v_z}{\partial\zeta\,\partial\eta}-2\frac{\eta}{R}\frac{\mathrm{d}R}{\mathrm{d}\zeta}\frac{\partial\mu}{\partial\eta}\frac{\partial v_z}{\partial\zeta}-\alpha\frac{\mu}{R}\frac{\mathrm{d}R}{\mathrm{d}\zeta}\frac{\partial v_z}{\partial\zeta}+2\left(\frac{\eta}{R}\frac{\mathrm{d}R}{\mathrm{d}\zeta}\right)^2\frac{\partial\mu}{\partial\eta}\frac{\partial v_z}{\partial\eta}\\&+\mu\left(\frac{\eta}{R}\frac{\mathrm{d}R}{\mathrm{d}\zeta}\right)^2\frac{\partial^2 v_z}{\partial\eta^2}+\frac{1}{R}\frac{\partial\mu}{\partial\eta}\frac{\partial v_r}{\partial\zeta}-\frac{\eta}{R^2}\frac{\mathrm{d}R}{\mathrm{d}\zeta}\frac{\partial\mu}{\partial\eta}\frac{\partial v_r}{\partial\eta}+\frac{\partial\mu}{\partial\zeta}\frac{\partial v_z}{\partial\zeta}+G_z\Bigg].\end{aligned}$$

NUMERICAL ANALYSIS

Grid and control volumes

The computational domain is divided into control volumes and the grid points are placed in the geometric centre of each control volume. The pressure variable is located on the central grid point whereas the velocity variables are located on the faces of the control volume. This forms a staggered grid system since the control volume associated with the velocity is staggered with respect to the pressure control volume as shown in Figure 2.

Conservation equation for the control volume

The discretized equations are derived by integrating the governing equations over the control volume. The final equations may be rearranged to the following form:

r-momentum

$$a^v_{\mathrm{P}_1}v_{r,\mathrm{P}_1}=a^v_{\mathrm{E}_1}v_{r,\mathrm{E}_1}+a^v_{\mathrm{W}_1}v_{r,\mathrm{W}_1}+a^v_{\mathrm{N}_1}v_{r,\mathrm{N}_1}+a^v_{\mathrm{S}_1}v_{r,\mathrm{S}_1}+A^v_{\mathrm{P}_1}(p_{\mathrm{s}_1}-p_{\mathrm{n}_1})+B^v_{\mathrm{P}_1}, \tag{18}$$

where

$$a^v_{\mathrm{P}_1}=a^v_{\mathrm{E}_1}+a^v_{\mathrm{W}_1}+a^v_{\mathrm{N}_1}+a^v_{\mathrm{S}_1},$$

$$a^v_{\mathrm{E}_1}=\frac{C_{\zeta,\mathrm{e}_1}\delta\eta_{\mathrm{N}}}{\delta\zeta_{\mathrm{E}}}, \qquad a^v_{\mathrm{W}_1}=\frac{C_{\zeta,\mathrm{w}_1}\delta\eta_{\mathrm{N}}}{\delta\zeta_{\mathrm{W}}}, \qquad a^v_{\mathrm{N}_1}=\frac{C_{\eta,\mathrm{n}_1}\Delta\zeta_{\mathrm{P}}}{\Delta\eta_{\mathrm{N}}}, \qquad a^v_{\mathrm{S}_1}=\frac{C_{\eta,\mathrm{s}_1}\Delta\zeta_{\mathrm{P}}}{\Delta\eta_{\mathrm{P}}}, \tag{19}$$

$$A^v_{\mathrm{P}_1}=\left(\frac{(\eta R)^\alpha}{R}\right)_{\mathrm{P}_1}\Delta\zeta_{\mathrm{P}}, \qquad B^v_{\mathrm{P}_1}=(S_\eta)_{\mathrm{P}_1}\Delta\zeta_{\mathrm{P}}\delta\eta_{\mathrm{N}};$$

z-momentum

$$a^u_{\mathrm{P}_2}v_{z,\mathrm{P}_2}=a^u_{\mathrm{E}_2}v_{z,\mathrm{E}_2}+a^u_{\mathrm{W}_2}v_{z,\mathrm{W}_2}+a^u_{\mathrm{N}_2}v_{z,\mathrm{N}_2}+a^u_{\mathrm{S}_2}v_{z,\mathrm{S}_2}+A^u_{\mathrm{P}_2}(p_{\mathrm{w}_2}-p_{\mathrm{e}_2})+B^u_{\mathrm{P}_2}, \tag{20}$$

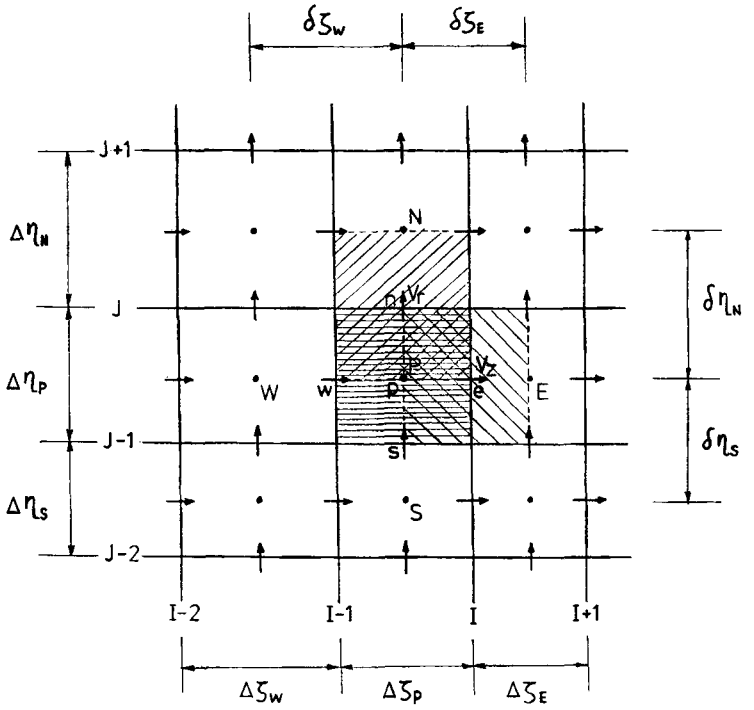

Figure 2. Grid and control volumes

where

$$a^u_{P_2}=a^u_{E_2}+a^u_{W_2}+a^u_{N_2}+a^u_{S_2},$$

$$a^u_{E_2}=\frac{C_{\zeta,e_2}\Delta\eta_P}{\Delta\zeta_E},\qquad a^u_{W_2}=\frac{C_{\zeta,w_2}\Delta\eta_P}{\Delta\zeta_P},\qquad a^u_{N_2}=\frac{C_{\eta,n_2}\delta\zeta_E}{\delta\eta_N},\qquad a^u_{S_2}=\frac{C_{\eta,s_2}\delta\zeta_E}{\delta\eta_S},\tag{21}$$

$$A^u_{P_2}=(\eta R)^\alpha_{P_2}\Delta\eta_P,\qquad B^u_{P_2}=(S_\zeta)_{P_2}\delta\zeta_E\Delta\eta_P.$$

Here the subscripts 1 and 2 refer to the control volume for the radial and axial momentum equations respectively.

The continuity equation in its integrated form can be written as

$$\{[(\eta R)^\alpha v_r]_n-[(\eta R)^\alpha v_r]_s\}\Delta\zeta_P+\{[(\eta R)^\alpha v_z]_e-[(\eta R)^\alpha v_z]_w\}\Delta\eta_P$$
$$-\left[\left((\eta R)^\alpha\eta\frac{dR}{d\zeta}v_z\right)_n-\left((\eta R)^\alpha\eta\frac{dR}{d\zeta}v_z\right)_s\right]\Delta\zeta_P=0.\tag{22}$$

This continuity equation plays an important role in relating the velocity terms to the pressure. The velocities may be corrected according to the constraint that the continuity equation must be satisfied at all times. The velocity correction equations can be derived in terms of pressure corrections by making use of the relationships

$$p=p^*+p',\qquad v_r=v_r^*+v_r',\qquad v_z=v_z^*+v_z',\tag{23}$$

where superscripts 'asterisk' and 'prime' denote the guessed and correction values respectively. Substituting (23) into the momentum equation and considering that the 'asterisked' terms satisfy the equation exactly gives

$$\begin{aligned} v'_{z,e} &= \frac{A^u_e}{a^u_e}(p'_P - p'_E) = d^u_e(p'_P - p'_E), \\ v'_{z,w} &= \frac{A^u_w}{a^u_w}(p'_W - p'_P) = d^u_w(p'_W - p'_P), \\ v'_{r,n} &= \frac{A^v_n}{a^v_n}(p'_P - p'_N) = d^v_n(p'_P - p'_N), \\ v'_{r,s} &= \frac{A^v_s}{a^v_s}(p'_S - p'_P) = d^v_s(p'_S - p'_P). \end{aligned} \tag{24}$$

The pressure correction equation is derived from the continuity equation in a similar fashion as

$$a^p_P p'_P = a^p_E p'_E + a^p_W p'_W + a^p_N p'_N + a^p_S p'_S + b^p_P, \tag{25}$$

where

$$a^p_P = a^p_E + a^p_W + a^p_N + a^p_S,$$

$$a^p_E = (\eta R)^\alpha_e R_e d^u_e \Delta\eta_P - \left((\eta R)^\alpha \eta \frac{dR}{d\zeta}\right)_n \frac{d^u_e \Delta\eta_N}{4\delta\eta_N}\Delta\zeta_P + \left((\eta R)^\alpha \eta \frac{dR}{d\zeta}\right)_s \frac{d^u_e \Delta\eta_S}{4\delta\eta_S}\Delta\zeta_P,$$

$$a^p_W = (\eta R)^\alpha_w R_w d^u_w \Delta\eta_P + \left((\eta R)^\alpha \eta \frac{dR}{d\zeta}\right)_n \frac{d^u_w \Delta\eta_N}{4\delta\eta_N}\Delta\zeta_P - \left((\eta R)^\alpha \eta \frac{dR}{d\zeta}\right)_s \frac{d^u_w \Delta\eta_S}{4\delta\eta_S}\Delta\zeta_P,$$

$$a^p_N = (\eta R)^\alpha_n d^v_n \Delta\zeta_P, \qquad a^p_S = (\eta R)^\alpha_s d^v_s \Delta\zeta_P,$$

$$\begin{aligned} b^p_P = &\left((\eta R)^\alpha \eta \frac{dR}{d\zeta}\right)_n \frac{\Delta\eta_P}{4\delta\eta_N}[d^u_{nw}(p'_{NW} - p'_N) + d^u_{ne}(p'_N - p'_{NE})]\Delta\zeta_P \\ &- \left((\eta R)^\alpha \eta \frac{dR}{d\zeta}\right)_s \frac{\Delta\eta_P}{4\delta\eta_S}[d^u_{sw}(p'_{SW} - p'_S) + d^u_{se}(p'_S - p'_{SE})]\Delta\zeta_P - m^*_P, \end{aligned}$$

$$\begin{aligned} m^*_P = &[(\eta R)^\alpha_n v^*_{r,n} - (\eta R)^\alpha_s v^*_{r,s}]\Delta\zeta_P + [(\eta R)^\alpha_e R_e v^*_{z,e} - (\eta R)^\alpha_w R_w v^*_{z,w}]\Delta\eta_P \\ &- \left[\left((\eta R)^\alpha \eta \frac{dR}{d\zeta}\right)_n v^*_{z,n} - \left((\eta R)^\alpha \eta \frac{dR}{d\zeta}\right)_s v^*_{z,s}\right]\Delta\zeta_P. \end{aligned} \tag{26}$$

According to the SIMPLER scheme, similar equations to those above are used to calculate the pressure terms. These are derived from the continuity and momentum equations in an identical fashion. From the momentum equation the velocities on the faces are given by

$$\begin{aligned} v_{z,e} &= \frac{a^u_{ee} v_{z,ee} + a^u_w v_{z,w} + a^u_{ne} v_{z,ne} + a^u_{se} v_{z,se} + B^u_e}{a^u_e} + d^u_e(p_P - p_E) \\ &= \hat{v}_{z,e} + d^u_e(p_P - p_E), \end{aligned} \tag{27}$$

etc. These expressions along with the continuity equation determine the discretized expression for the pressure as

$$a_P^p p_P = a_E^p p_E + a_W^p p_W + a_N^p p_N + a_S^p p_S + B_P^p, \tag{28}$$

where

$$\begin{aligned} B_P^p = & \left((\eta R)^\alpha \eta \frac{dR}{d\zeta}\right)_n \frac{\Delta\eta_P}{4\delta\eta_N}\left[d_{nw}^u(p_{NW}-p_N)+d_{ne}^u(p_N-p_{NE})\right]\Delta\zeta_P \\ & -\left((\eta R)^\alpha \eta \frac{dR}{d\zeta}\right)_s \frac{\Delta\eta_P}{4\delta\eta_S}\left[d_{sw}^u(p_{SW}-p_S)+d_{se}^u(p_S-p_{SE})\right]\Delta\zeta_P - \hat{m}_P, \\ \hat{m}_P = & \left[(\eta R)_n^\alpha \hat{v}_{r,n} - (\eta R)_s^\alpha \hat{v}_{r,s}\right]\Delta\zeta_P + \left[(\eta R)_e^\alpha R_e \hat{v}_{z,e} - (\eta R)_w^\alpha R_w \hat{v}_{z,w}\right]\Delta\eta_P \\ & -\left[\left((\eta R)^\alpha \eta \frac{dR}{d\zeta}\right)_n \hat{v}_{z,n} - \left((\eta R)^\alpha \eta \frac{dR}{d\zeta}\right)_s \hat{v}_{z,s}\right]\Delta\zeta_P. \end{aligned} \tag{29}$$

The boundary conditions on the free surface can be formulated explicitly as

$$\frac{\partial v_r}{\partial \eta} = \frac{dR}{d\zeta}\frac{\partial v_z}{\partial \eta} + \frac{R}{2\mu\left[1+(dR/d\zeta)^2\right]}\left\{2\mu\frac{dR}{d\zeta}\frac{\partial v_r}{\partial \zeta} - 2\mu\left(\frac{dR}{d\zeta}\right)^2\frac{\partial v_z}{\partial \zeta} + (p-p_a-HS)\left[1+\left(\frac{dR}{d\zeta}\right)^2\right]\right\}, \tag{30}$$

$$\frac{\partial v_z}{\partial \eta} = -\frac{dR}{d\zeta}\frac{\partial v_r}{\partial \eta} + \frac{R}{1+(dR/d\zeta)^2}\left\{2\frac{dR}{d\zeta}\frac{\partial v_z}{\partial \zeta} - \left[1-\left(\frac{dR}{d\zeta}\right)^2\right]\frac{\partial v_r}{\partial \zeta}\right\}. \tag{31}$$

These two equations are interchangeably used to eliminate the radial gradient term on the right-hand side of each equation, which then results in the following form for the boundary conditions:

$$\frac{\partial v_r}{\partial \eta} = \frac{R(dR/d\zeta)^3}{\left[1+(dR/d\zeta)^2\right]^2}\frac{\partial v_r}{\partial \zeta} + \frac{R(dR/d\zeta)^2}{\left[1+(dR/d\zeta)^2\right]^2}\frac{\partial v_z}{\partial \zeta} + \frac{R}{2\mu\left[1+(dR/d\zeta)^2\right]}(p-p_a-HS), \tag{32}$$

$$\frac{\partial v_z}{\partial \eta} = \frac{R(dR/d\zeta)\left[2+(dR/d\zeta)^2\right]}{\left[1+(dR/d\zeta)^2\right]^2}\frac{\partial v_z}{\partial \zeta} - \frac{R}{\left[1+(dR/d\zeta)^2\right]^2}\frac{\partial v_r}{\partial \zeta} - \frac{R(dR/d\zeta)}{2\mu\left[1+(dR/d\zeta)^2\right]}(p-p_a-HS). \tag{33}$$

The first terms on the right-hand side of these expressions are discretized and combined with the radial and axial momentum equations respectively to give the following discretized expressions on the free boundary control volume:

$$\begin{aligned} \left(a_{P_1}^v + \frac{C_{\eta,n_1}R_{n_1}(dR/d\zeta)_{n_1}^3}{\left[1+(dR/d\zeta)_{n_1}^2\right]^2}\frac{1-b}{b}\frac{\Delta\zeta_P}{\delta\zeta_W}\right)v_{r,P_1} = & \left(a_{E_1}^v + \frac{C_{\eta,n_1}R_{n_1}(dR/d\zeta)_{n_1}^3}{\left[1+(dR/d\zeta)_{n_1}^2\right]^2}\frac{1}{b(b+1)}\frac{\Delta\zeta_P}{\delta\zeta_W}\right)v_{r,E_1} \\ & + \left(a_{W_1}^v + \frac{C_{\eta,n_1}R_{n_1}(dR/d\zeta)_{n_1}^3}{\left[1+(dR/d\zeta)_{n_1}^2\right]^2}\frac{b}{b+1}\frac{\Delta\zeta_P}{\delta\zeta_W}\right)v_{r,W_1} + a_{S_1}^v v_{r,S_1} \\ & + A_{P_1}^v(p_{s_1}-p_{n_1}) + B_{P_1}^v + \frac{C_{\eta,n_1}R_{n_1}(dR/d\zeta)_{n_1}^2}{\left[1+(dR/d\zeta)_{n_1}^2\right]^2}\Delta\zeta_P\left(\frac{\partial v_z}{\partial \zeta}\right)_{n_1} \\ & + \frac{C_{\eta,n_1}R_{n_1}\Delta\zeta_P}{2\mu\left[1+(dR/d\zeta)_{n_1}^2\right]}(p-p_a-HS)_{n_1}, \end{aligned} \tag{34}$$

$$\left(a^u_{P_2}+\frac{C_{\eta,n_2}R_{n_2}(dR/d\zeta)_{n_2}[2+(dR/d\zeta)^2_{n_2}]}{[1+(dR/d\zeta)^2_{n_2}]^2}\frac{1-a}{a}\frac{\delta\zeta_E}{\delta\zeta_P}\right)v_{z,P_2}$$
$$=\left(a^u_{E_2}+\frac{C_{\eta,n_2}R_{n_2}(dR/d\zeta)_{n_2}[2+(dR/d\zeta)^2_{n_2}]}{[1+(dR/d\zeta)^2_{n_2}]^2}\frac{1}{a(a+1)}\frac{\delta\zeta_E}{\Delta\zeta_P}\right)v_{z,E_2}$$
$$+\left(a^u_{W_2}+\frac{C_{\eta,n_2}R_{n_2}(dR/d\zeta)_{n_2}[2+(dR/d\zeta)^2_{n_2}]}{[1+(dR/d\zeta)^2_{n_2}]^2}\frac{a}{a+1}\frac{\delta\zeta_E}{\Delta\zeta_P}\right)v_{z,W_2}+a^u_{S_2}v_{z,S_2}$$
$$+A^u_{P_2}(p_{w_2}-p_{e_2})+B^u_{P_2}-\frac{C_{\eta,n_2}R_{n_2}}{[1+(dR/d\zeta)^2_{n_2}]^2}\delta\zeta_E\left(\frac{\partial v_r}{\partial\zeta}\right)_{n_2}$$
$$-\frac{C_{\eta,n_2}R_{n_2}(dR/d\zeta)_{n_2}\delta\zeta_E}{2\mu[1+(dR/d\zeta)^2_{n_2}]}(p-p_a-HS)_{n_2}, \tag{35}$$

where $a=\Delta\zeta_E/\Delta\zeta_P$ and $b=\delta\zeta_E/\delta\zeta_W$. Again the continuity equation can be integrated on the free surface to give the discretized equation, and after some manipulation with equations (32) and (33), yields an expression for calculation of the pressure on the free surface:

$$0=\left[R_e^{\alpha+1}-\frac{\alpha+1}{2}R_P^\alpha\left(\frac{dR}{d\zeta}\right)_P\Delta\zeta_P-\frac{R_P^{\alpha+1}(dR/d\zeta)_P^2}{1+(dR/d\zeta)_P^2}\right]v_{z,e}$$
$$-\left[R_w^{\alpha+1}+\frac{\alpha+1}{2}R_P^\alpha\left(\frac{dR}{d\zeta}\right)_P\Delta\zeta_P-\frac{R_P^{\alpha+1}(dR/d\zeta)_P^2}{1+(dR/d\zeta)_P^2}\right]v_{z,w}$$
$$+\left[\alpha R_P^\alpha\Delta\zeta_P+\frac{R_P^{\alpha+1}(dR/d\zeta)_P}{1+(dR/d\zeta)_P^2}\left(\frac{\Delta\zeta_E}{2\delta\zeta_E}-\frac{\Delta\zeta_W}{2\delta\zeta_W}\right)\right]v_{r,P}$$
$$+\frac{R_P^{\alpha+1}(dR/d\zeta)_P}{1+(dR/d\zeta)_P^2}\frac{\Delta\zeta_P}{2\delta\zeta_E}v_{r,E}-\frac{R_P^{\alpha+1}(dR/d\zeta)_P}{1+(dR/d\zeta)_P^2}\frac{\Delta\zeta_P}{2\delta\zeta_W}v_{r,W}$$
$$+\frac{R_P^{\alpha+1}}{2\mu}\Delta\zeta_P(p-p_a-HS)_P. \tag{36}$$

All derivatives which appear in the source terms and the equations developed above are discretized with second-order accuracy, $O(\Delta^2)$.

Solution procedure

The computation procedure is given by the following sequence.

1. Guess a velocity field.
2. Compute the free boundary shape from the no-penetration boundary condition $\mathbf{v}\cdot\mathbf{n}=0$ by using Simpson's rule:

$$R_i=R_{i-1}+\int_{z_{i-1}}^{z_i}\frac{v_{r,i}}{v_{z,i}}\,dz.$$

3. Calculate the coefficients in the momentum and pressure equations.
4. Compute the free boundary pressure and velocities from (34)–(36).
5. Compute $\hat{v}_r$ and $\hat{v}_z$ from expressions such as (27) by substituting values of the neighbouring velocities.
6. Evaluate the mass source term B_P^p from (29) and solve (28) to obtain the pressure field p.

7. Regarding the pressure field as p^*, the momentum equations (18) and (20) are solved to obtain v_r^* and v_z^*.
8. Calculate the mass source term b_P^p from (26) and solve (25) to obtain the pressure correction field p'.
9. Using the p'-field, correct the 'asterisked' velocities by means of (23) and (24). The pressure is not corrected.
10. Return to step 5 with the corrected velocity field and repeat the procedure until the inner domain variables converge within the tolerable error bound $\varepsilon = 10^{-3}$.
11. Return to step 4 to update the free boundary pressure and velocities and repeat until they converge within $\varepsilon = 10^{-3}$.
12. Once the field variables have been computed, return to step 2 so that the free surface shape is updated and the steps outlined above will be repeated until the surface shape converges within a tolerable error bound, which is set as $\varepsilon = 0{\cdot}5 \times 10^{-3}$.

This problem is solved by the so-called 'line-by-line technique' and the resulting tridiagonal matrix is solved using the Thomas algorithm. The calculated fields are underrelaxed by a factor of 0·2 and the free surface shape is underrelaxed by a factor of 0·4. The additive correction methods, which are described by Settari and Aziz[34] and called the block correction procedure by Patankar,[35] are known to increase the speed of convergence of the line-by-line technique. In the simulation of extrudate swell, owing to the stress singularity at the die exit, the computed field of each variable is very sensitive to the computed field of the other variables from the previous iteration, so that the computation may proceed to a solution which does not satisfy the momentum balance and accordingly may give an irregular shape for the free surface. However, if the additive correction method is applied to the z-momentum and pressure correction equations, these anomalies can be eliminated. The inner loops of the z-momentum and pressure correction equations are cycled for six iterations each. Application of the additive correction approach to the third and sixth iteration is sufficient to overcome these difficulties and the computation converges in a desirable manner to give the free surface shape and the detailed flow field.

RESULTS AND DISCUSSION

In principle, the domain of interest for the extrudate swell problem must be infinite in extent in order to apply the theoretical boundary conditions far upstream and downstream of the die exit. However, previous numerical calculations by Nickell *et al.*[4] and Dutta and Ryan[33] and experimental investigations by Gottlieb and Bird,[36] Whipple and Hill[37] and Higashitani *et al.*[38] indicate that the exit region lies approximately within distances of about half of the die opening both upstream and downstream from the exit plane. Accordingly, the computational domain is restricted to lie within $\zeta = -3$ and $\zeta = 3$. This does not pose any problem when there are no gravity effects. However, with gravity, a sufficiently long downstream domain is needed in order to avoid a contradiction of the calculated pressure field as a result of applying the present boundary condition at a finite distance.[39] The computational domain is then discretized into an $I \times J$ non-uniform grid, I and J being the numbers of discrete nodes in ζ- and η-direction respectively.

Effect of mesh refinement

In order to evaluate the effectiveness of the numerical scheme, the Newtonian jet swell problem was first solved by neglecting the gravitational and surface tension effects. The computations were performed on three different meshes in order to select an optimum grid for further calculations. These meshes are illustrated in Figure 3 and the corresponding results in Table I show that as the

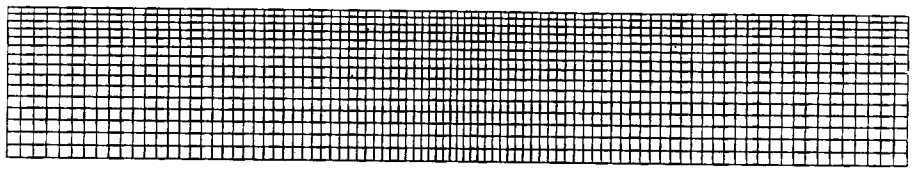

90 × 15(a)

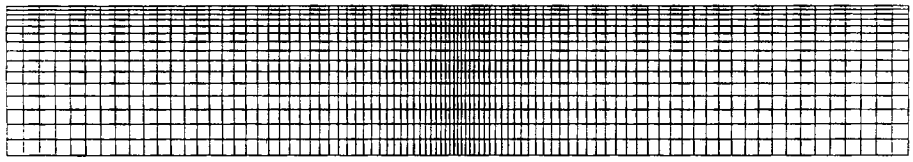

90 × 15(b)

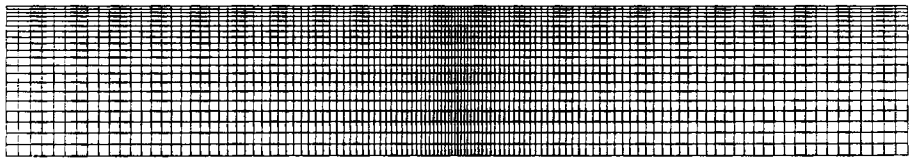

120 × 20(c)

Figure 3. Meshes tested in the calculations

Table I. Effect of mesh refinement on extrudate swell and the variables at the die lip ($S=0$, $G=0$)

	Axisymmetric, $\alpha=1$		
	90 × 15 (a)	90 × 15 (b)	120 × 20 (c)
% swell	14·94	13·23	13·11
p	−13·323	−19·027	−21·739
τ_{rr}	−6·964	−9·935	−11·501
τ_{zz}	19·760	28·103	32·112
τ_{rz}	−11·626	−15·738	−17·911
E	0·0234	0·0061	0·0026
CPU time (min)	17	26	117
	Planar, $\alpha=0$		
	90 × 15 (a)	90 × 15 (b)	120 × 20 (c)
% swell	21·35	19·16	19·14
p	−12·073	−17·028	−19·475
τ_{rr}	−6·365	−8·925	−10·277
τ_{zz}	18·456	25·550	29·194
τ_{rz}	−10·428	−14·002	−15·922
E	0·0257	0·0022	0·0002
CPU time (min)	16	48	81

grid size is refined, the extent of swell decreases to a value which is not affected by any further change in grid structure. However, the computational cost increases substantially as the number of grid points increases. On a VAX 8820 machine, grid type (b) requires 26 min of CPU time while type (c) requires 117 min of CPU time for the axisymmetric case.

The mass must be conserved at any location along the flow. Since a fully developed velocity profile whose average is unity is assigned at the far upstream boundary, the mass flow rate across any cross-sectional area to the stream should be equal to that at the far upstream boundary. The error in the mass conservation is calculated by the equation

$$E = \int_{A_i} (2\pi r)^{\alpha} v_z \, dr - \int_{A_f} (2\pi r)^{\alpha} v_z \, dr, \tag{37}$$

where A_i and A_f are the cross-sectional areas of the upstream and downstream boundaries respectively. The values of E for each grid type are also shown in Table I. Here we can see that the more refined mesh satisfies continuity much better. According to these observations, grid type (b) was selected as the optimum grid and used in all calculations reported subsequently.

Analysis of the stick–slip problem for axisymmetric dies

The results of the extrudate swell problem are better understood by first analysing a stick–slip problem with respect to the stress singularity and the flow rearrangement which occurs near the exit plane. The boundary conditions for this problem are such that for $\zeta < 0$ the no-slip condition is valid, whereas for $\zeta > 0$ a zero-shear-stress condition is applied. The first successful attempt to analyse this problem was made by Richardson[9,10] for the planar stick–slip case. The axisymmetric stick–slip problem was analyzed by Trogdon and Joseph.[11] Similar analyses have been reported by Coleman[40] for second-order fluids and by Vrentas and Duda.[41] They found that there is a square root singularity near the exit lip and the flow rearrangement is completed within a distance of about half of the die opening both upstream and downstream from the exit plane. Apart from the absence of a curved free surface, the stick–slip problem resembles the extrudate swell problem in many respects, particularly with regard to the stress singularities resulting from the presence of mixed boundary conditions.[9,10,42,43] The solution of the stick–slip problem is important in two major respects. Firstly, the validity of the numerical scheme can be effectively tested by comparison with analytical results. Secondly, the solution of the stick–slip problem serves as an excellent initial guess for the extrudate swell calculations. The numerical scheme developed here was tested by comparing the numerical results of the axisymmetric stick–slip case with the analytical solution given by Trogdon and Joseph.[11] The velocity profiles given in Figures 4 and 5 show excellent agreement with the analytical solution which is obtained by using up to 100 terms in the series expansion.

According to Richardson,[9] the surface velocity can be expressed in the form $v_s = Az^b$, where $A = 1{\cdot}162$ and $b = 0{\cdot}50$ for a slit die as z approaches zero. Also, Chang *et al.*[44] indicated that the integrated total axial stress on the die exit plane must be equal to zero, since at zero Reynolds number an integral momentum balance gives

$$I = \int_0^1 r^{\alpha} \sigma_{zz} \, dr = 0. \tag{38}$$

This integral balance can be used for partially checking the accuracy of the calculations. Since the planar and cylindrical stick–slip cases have been considered by several investigators, the results are compared between different solutions in Table II. The present data for A and b were obtained by linear regression of the first five node point velocities from the die exit. The results are in

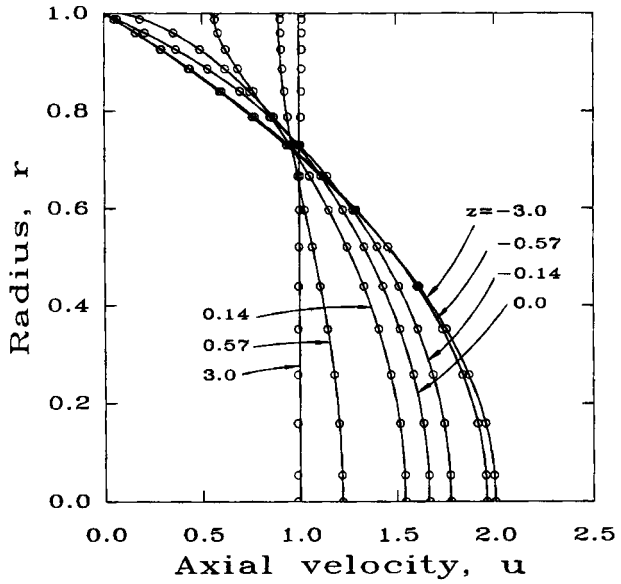

Figure 4. Axial velocity profiles for stick–slip problem—comparison between present scheme and analytical solution, axisymmetric case, $\alpha = 1$: ○, present scheme; ——, analytical solution

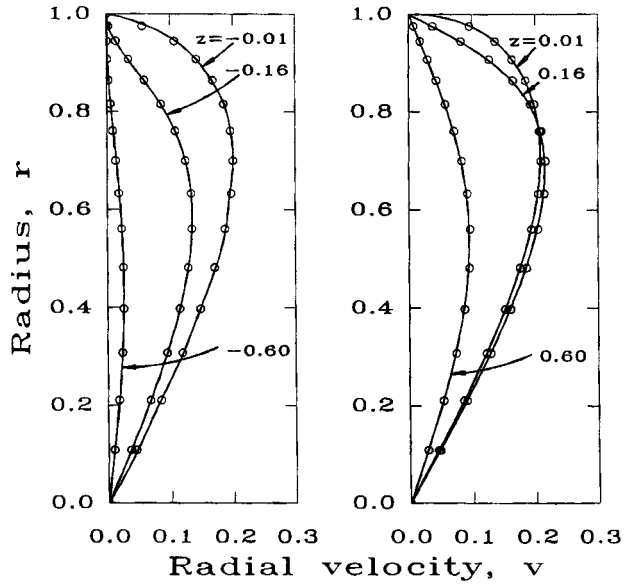

Figure 5. Radial velocity profiles for stick–slip problem—comparison between present scheme and analytical solution, axisymmetric case, $\alpha = 1$: ○, present scheme; ——, analytical solution

Table II. Comparison of stick–slip results

	Planar, $\alpha=0$					Axisymmetric, $\alpha=1$	
		Chang *et al.*[44]					
	Richardson[9] exact solution	Collocation 3 × 10	Galerkin 3 × 9	Dutta[45] FDM	Present work	Dutta[45] FDM	Present work
A	1·162	—	—	1·170	1·120	1·243	1·233
b	0·50	0·37	0·43	0·466	0·436	0·436	0·414
I	0·0	0·000018	−0·206	−0·0115	−0·0158	0·0003	−0·0041
$p(0, 0)$	1·04	0·962	1·110	1·002	1·100	2·24	2·30
$p_{w,s}$	0·81	0·844	0·842	0·792	1·081	1·38	1·97
e	0·135	0·141	0·140	0·132	0·180	0·1725	0·246

reasonably good agreement with those obtained using different solution techniques. The data for the integral balance are small enough to ensure the accuracy of the present numerical scheme.

The term $p_{w,s}$ denotes the wall pressure extrapolated from upstream to the die exit. The quantity $e=p_{w,s}/2\tau_w$ is the equivalent length of the exit pressure losses. The present scheme shows somewhat higher values for this equivalent length than the other solutions.

Figures 6(a) and 6(b) give the pressure profiles along the symmetric axis and the stick–slip surface for the cylindrical and planar cases respectively. The axial pressure gradient along the centreline decreases monotonically from the Poiseuille value of -8 or -3 (for $\alpha=1$ or 0) to zero as the fluid traverses through the exit region. The surface pressure, on the other hand, shows a negative value at the die exit and asymptotically approaches zero far downstream. This behaviour at the exit is predicted to be a square root singularity from the analytical solution. In addition, the results agree reasonably well with values previously reported by other authors, except in the immediate vicinity of the die exit where Chang *et al.*'s data show a pulse to a higher positive value and then a drop to a negative value. This pulse in the wall pressure at the die exit is commonly detected in finite element calculations. In this work, however, it was not detected by the present scheme since zero radial pressure gradient is applied on the wall because of the known velocity boundary condition. Dutta's[45] finite difference scheme also did not show the pulse at the exit.

For the axisymmetric case the results for the velocity, pressure and stress fields are given in Figures 7(a)–7(e). In Figure 7(a) it can be seen that the rapid rearrangement of the flow regime is essentially confined to lie within half of the die opening both upstream and downstream from the exit plane. Figures 7(b)–7(e) show the pressure and stress singularities at the die exit. The radial stress exhibits only a compressive force at the exit, whereas the axial stress exhibits both a highly tensile force at the exit lip and a compressive force near the centreline of the exit plane. This is a result of the fact that the total axial load is zero when the Reynolds number is zero, as indicated by Chang *et al.*[44] The shear stress at the wall far inside the tube is -4, which is the same as that predicted by the swell calculations of Nickell *et al.*[4] and Dutta and Ryan.[33]

Jet swell without gravity and surface tension

Figure 8 shows the free jet profile for a cylindrical jet in the absence of surface tension and gravity. A swelling ratio of 13·23% is predicted by the present numerical scheme for the

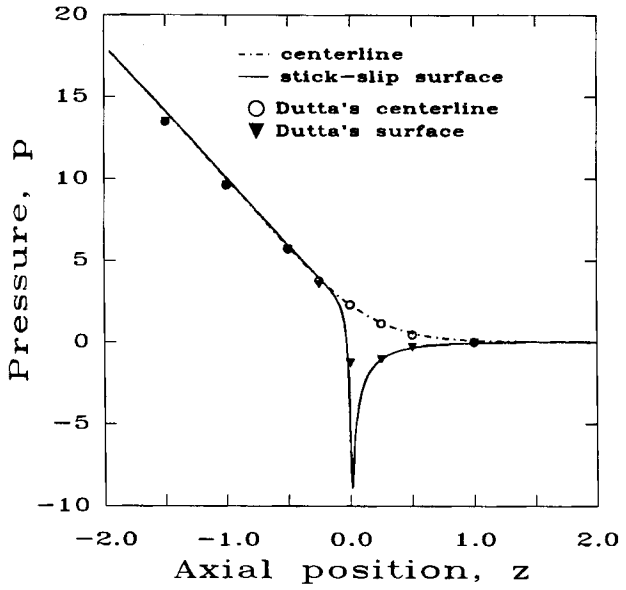

Figure 6(a). Pressure profiles for stick–slip problem, axisymmetric case, $\alpha = 1$

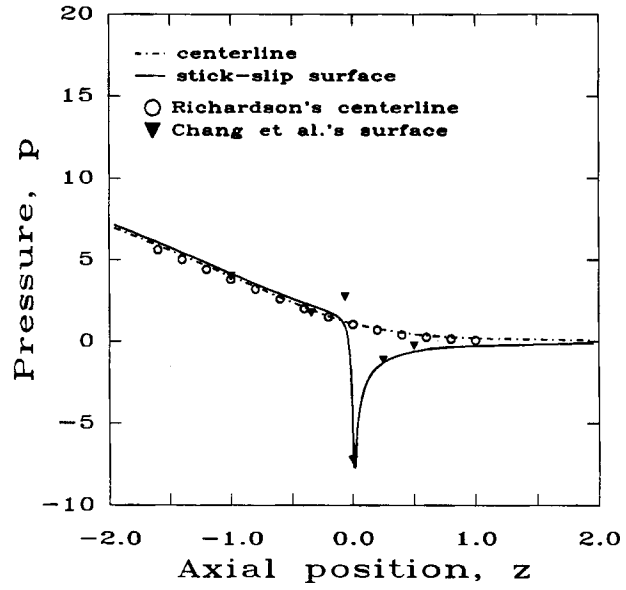

Figure 6(b). Pressure profiles for stick–slip problem, planar case, $\alpha = 0$

axisymmetric jet, which is in reasonably close agreement with the available experimental observations and other previous numerical predictions. The experimental measurements of Batchelor *et al.*[3] ahd Nickell *et al.*[4] give a swelling ratio of about 13·5% and the numerical results available from the literature range from 12%,[33] 12·6%,[25] 12·8%[4] and up to 13·0%.[17] The surface profiles for a plane jet are illustrated in Figure 9. The planar case has a swelling ratio of 19·6% and is

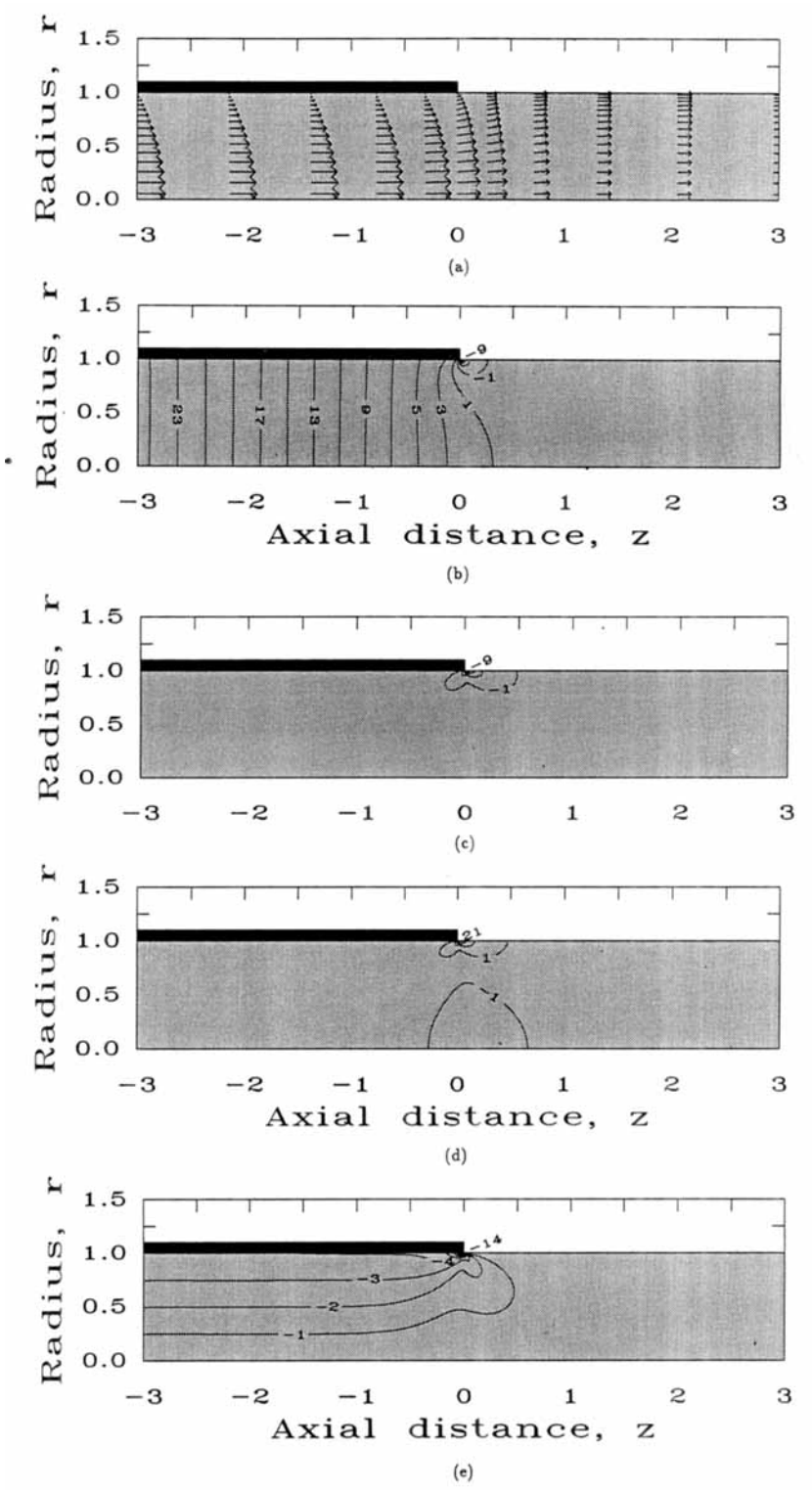

Figure 7. Contour plots for stick–slip problem, axisymmetric case, $\alpha = 1$: (a) velocity; (b) pressure; (c) radial extra stress τ_{rr}; (d) axial extra stress τ_{zz}; (e) shear stress τ_{rz}

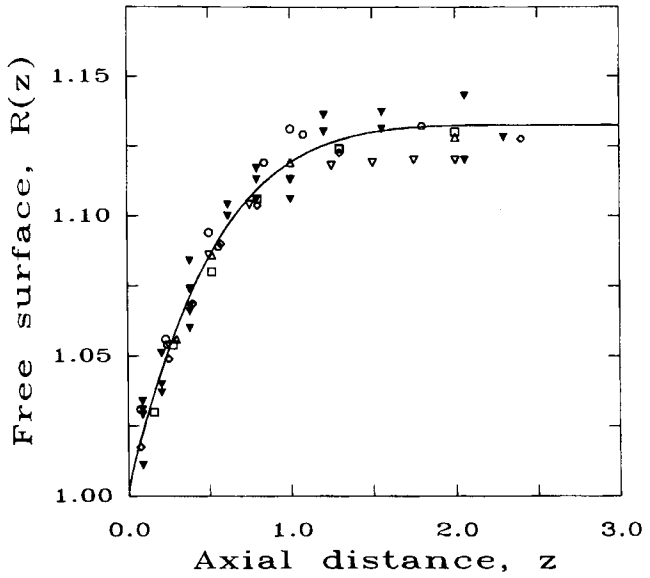

Figure 8. Comparison between numerical and experimental surface profiles for cylindrical jets, $S=0$, $G=0$. Numerical: ——, present work; △, Nickell *et al.*;[4] ○, Chang *et al.*,[24] Galerkin, 3 × 9 elements; □, Omodei;[17] ◇, Crochet and Keunings;[25] ▽, Dutta and Ryan.[33] Experimental: ▼, Batchelor *et al.*[3] for Paralac 385, a modified alkyd resin, $Re<10^{-8}$; ⬡, Nickell *et al.*[4] for silicone oil, $Re<10^{-3}$

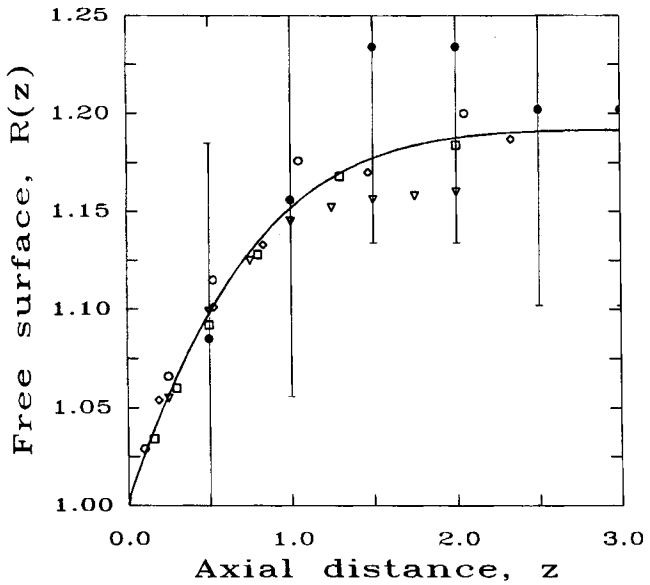

Figure 9. Comparison between numerical and experimental surface profiles for plane jets, $S=0$, $G=0$. Numerical: ——, present work; ○, Chang *et al.*,[24] Galerkin, 3 × 9 elements; □, Omodei;[17] ◇, Crochet and Keunings;[25] ▽, Dutta and Ryan.[33] Experimental: ⧫, Whipple and Hill[37] for silicone oil, $Re=3{\cdot}5\times10^{-4}$

considered to be in reasonable agreement with the experiments of Whipple and Hill[37] and the previous numerical predictions of 16·10%,[33] 16·58%,[24] 18·8%,[25] 19·0%[16] and 19·6%.[19] The flow and stress fields are plotted in Figures 10(a)–10(e). It can be seen that the pressure and axial stress singularities are more severe than in the stick–slip case. It is interesting to note, however, that the radial stress is alleviated in compressive force, whereas a small tensile force appears near the centreline in contrast to the stick–slip problem. For a plane jet the qualitative aspects of the flow field were found to be almost identical to those for the axisymmetric case and hence will not be discussed in detail here.

In Figure 11 the effect of shear thinning is shown to reduce the degree of swelling, which is in agreement with the calculations of Tanner *et al.*,[13] Boger *et al.*,[46] Coleman,[47] Mitsoulis *et al.*[19] and McClelland and Finlayson.[48] As mentioned by Mitsoulis *et al.*,[19] there exists a small contraction immediately after the exit for highly shear-thinning fluids ($n=0{\cdot}2$).

Effect of gravity

The influence of a gravitational field on the jet shape has been discussed by Dutta and Ryan,[33] who also used a finite difference numerical technique. The influence of a gravitational body force has been measured experimentally by Adachi and Yoshioka.[49] The final shape of the jet is a result of a dynamic balance between the competing influences of viscous and gravitational forces. Figure 12 shows the calculation results from the present work as compared with the previously mentioned studies. The numerical calculations of Dutta and Ryan show a large discrepancy with the data reported by Adachi and Yoshioka, whereas the present calculations are in much closer agreement. The discrepancy between the experiments and the calculational results arises from the imposition of an inadequate boundary condition far downstream. As discussed by Fischer *et al.*,[50] the overall length of the jet affects the velocity field and the final shape of the jet. The uniform axial velocity and zero-vorticity or zero-stress conditions far downstream result in a linear increase of pressure in the flow direction which is in contradiction with the uniform zero-pressure condition in the absence of surface tension and ambient pressure.[39] Therefore the jet length must be sufficiently long in order to apply the present boundary conditions, or alternatively the boundary conditions suggested by Adachi[51] have to be applied at a finite distance.

Effect of surface tension

Figure 13 shows the effect of surface tension on the shape of a capillary jet for different values of the surface tension parameter S, which is a measure of the ratio of surface tension to viscous forces. As with other previous numerical predictions,[15–17,33] surface tension inhibits jet swell owing to the inherent inward normal force on the free surface.

CONCLUSIONS

The results demonstrate the capability of employing a finite difference numerical method for solving the free surface extrudate swell problem by direct solution of the continuity and Cauchy momentum equations using velocity and pressure as the primitive variables. The method has been successfully applied to Newtonian and power-law fluid jets without any difficulty in accommodating the free surface by employing a staggered control volume grid. The finite difference technique involving co-ordinate transformation is able to approach the boundary generality of the finite element method. Although the application of the boundary conditions and the derivation and manipulation of the co-ordinate transformation are inherent disadvantages of the finite difference approach as compared to the use of finite elements for free surface problems,

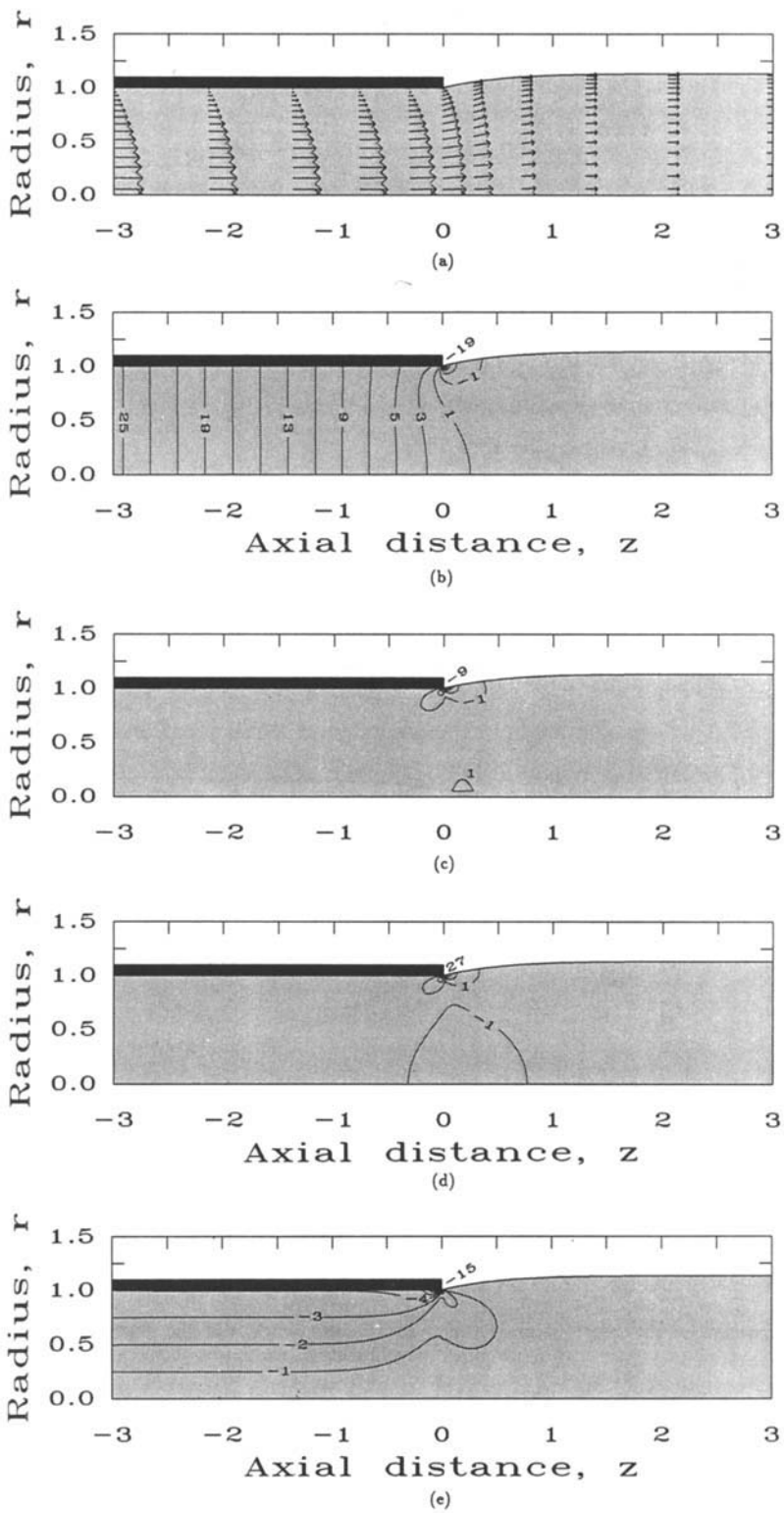

Figure 10. Contour plots for the Newtonian extrudate swell, axisymmetric case, $\alpha = 1$: (a) velocity; (b) pressure; (c) radial extra stress τ_{rr}; (d) axial extra stress τ_{zz}; (e) shear stress τ_{rz}

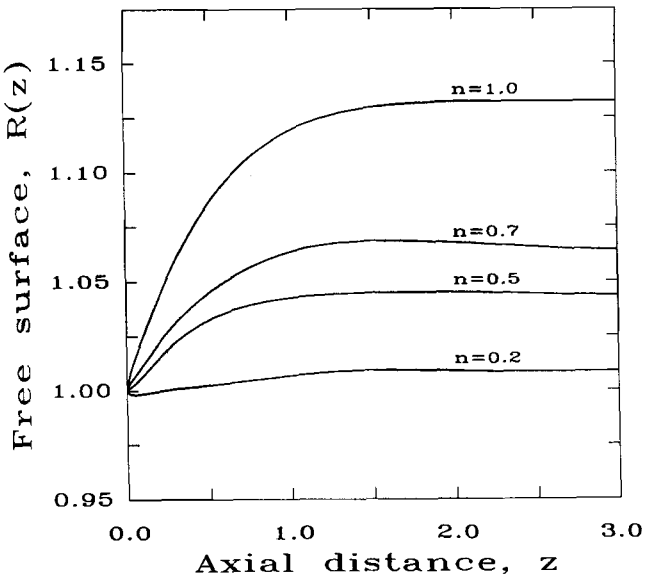

Figure 11. Free surface profiles for power-law fluids, axisymmetric case, $\alpha = 1$

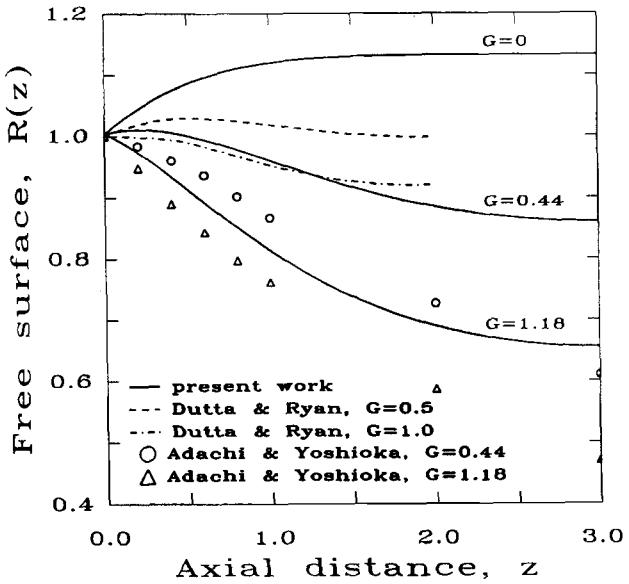

Figure 12. Comparison of the effect of gravity between present work and the experimental data of Adachi and Yoshioka,[49] axisymmetric case, $\alpha = 1$

the additional effort and complexity involved are not very demanding. The finite difference approach has some positive benefit with regard to the relative ease of mesh refinement. The computational efficiency of the present line-by-line overrelaxation scheme could be improved by implementing an efficient matrix inversion method and solving over the entire domain.

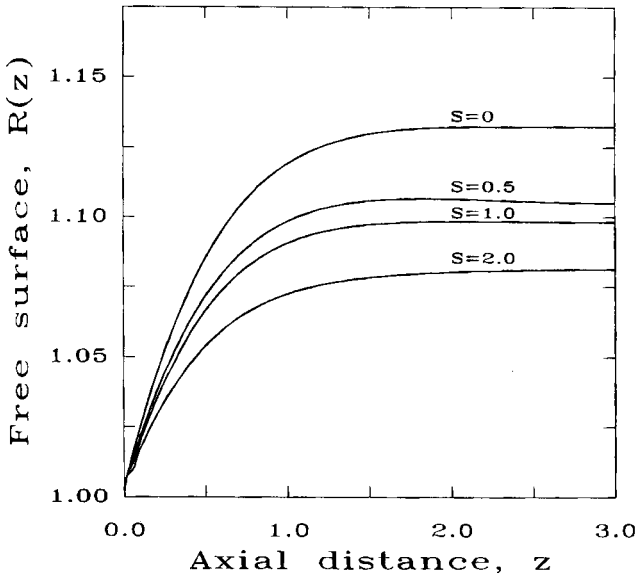

Figure 13. Effect of surface tension on a capillary jet, $\alpha = 1$

Even though finite element methods are almost exclusively employed for the solution of free surface fluid mechanics problems and attention to finite difference procedures has been virtually abandoned, the present study indicates that finite difference methods can be employed without formidable difficulty or complexity and that the method approaches the boundary generality of the finite element method.

REFERENCES

1. S. Middleman and J. Gavis, 'Expansion and contraction of capillary jets of Newtonian liquids', *Phys. Fluids*, **4**, 355 (1961).
2. S. L. Goren and S. Wronski, 'The shape of low-speed capillary jets of Newtonian liquids', *J. Fluid Mech.*, **25**, 185 (1966).
3. J. J. Batchelor, P. Berry and F. Horsfall, 'Die swell in elastic and viscous fluids', *Polymer*, **14**, 297 (1973).
4. R. E. Nickell, R. I. Tanner and B. Caswell, 'The solution of viscous incompressible jet and free-surface flows using finite-element methods', *J. Fluid Mech.*, **65**, 189 (1974).
5. R. L. Gear, M. Keentok, J. F. Milthorpe and R. I. Tanner, 'The shape of low Reynolds number jets', *Phys. Fluids*, **26**, 7 (1983).
6. W. W. Graessley, S. D. Glasscock and R. L. Crawley, 'Die swell in molten polymers', *Trans. Soc. Rheol.*, **14**, 519 (1970).
7. L. A. Utracki, Z. Bakerdjian and M. R. Kamal, 'A method for the measurement of true die swell of polymer melts', *J. Appl. Polym. Sci.*, **19**, 481 (1975).
8. D. C. Huang and J. L. White, 'Extrudate swell from slit and capillary dies: an experimental and theoretical study', *Polym. Eng. Sci.*, **19**, 609 (1979).
9. S. Richardson, 'A stick–slip problem related to the motion of a free jet at low Reynolds number', *Proc. Camb. Phil. Soc.*, **67**, 477 (1970).
10. S. Richardson, 'The die swell phenomenon', *Rheol. Acta*, **9**, 193 (1970).
11. S. A. Trogdon and D. D. Joseph, 'The stick–slip problem for a round jet: I. Large surface tension', *Rheol. Acta*, **19**, 404 (1980).
12. L. D. Sturges, 'A theoretical study of extrudate swell', *J. Non-Newtonian Fluid Mech.*, **9**, 357 (1981).
13. R. I. Tanner, R. E. Nickell and R. W. Bilger, 'Finite-element methods for the solution of some incompressible non-Newtonian fluid mechanics problems with free surfaces', *Comput. Methods Appl. Mech. Eng.*, **6**, 155 (1975).
14. W. Allan, 'Numerical die-swell evaluation for axisymmetric tube exits using finite element method', *Int. j. numer. methods eng.*, **11**, 1621 (1977).
15. K. R. Reddy and R. I. Tanner, 'Finite-element solution of viscous jet flows with surface tension', *Comput. Fluids*, **6**, 83 (1978).

16. B. J. Omodei, 'Computer solutions of a plane Newtonian jet with surface tension', *Comput. Fluids*, **7**, 79 (1979).
17. B. J. Omodei, 'On the die swell of an axisymmetric Newtonian jet', *Comput. Fluids*, **8**, 275 (1980).
18. K. J. Ruschak, 'A method for incorporating free boundaries with surface tension in finite element fluid-flow simulators', *Int. j. numer. methods eng.*, **15**, 639 (1980).
19. E. Mitsoulis, J. Vlachopoulos and F. A. Mirza, 'Numerical simulation of entry and exit flows in slit dies', *Polym. Eng. Sci.*, **24**, 707 (1984).
20. E. Mitsoulis, 'Extrudate swell in double-layer flows', *J. Rheol.*, **30**, S23 (1986).
21. G. C. Georgiou, T. C. Papanastasiou and J. O. Wilkes, 'Laminar Newtonian jets at high Reynolds number and high surface tension', *AIChE J.*, **34**, 1559 (1988).
22. A. Karagiannis, A. N. Hrymak and J. Vlachopoulos, 'Three-dimensional extrudate swell of creeping Newtonian jets', *AIChE J.*, **34**, 2088 (1988).
23. K. R. Reddy and R. I. Tanner, 'On swelling of extruded plane sheets', *J. Rheol.*, **22**, 661 (1978).
24. P.-W. Chang, T. W. Patten and B. A. Finlayson, 'Collocation and Galerkin finite-element methods for viscoelastic fluid flow—II', *Comput. Fluids*, **7**, 285 (1979).
25. M. J. Crochet and R. Keunings, 'Die swell of a Maxwell fluid: numerical prediction', *J. Non-Newtonian Fluid Mech.*, **7**, 199 (1980).
26. M. J. Crochet and R. Keunings, 'Finite element analysis of die swell of a highly elastic fluid', *J. Non-Newtonian Fluid Mech.*, **10**, 339 (1982).
27. C. J. Coleman, 'A finite element routine for analysing non-Newtonian flows, Part II: The extrusion of a Maxwell fluid', *J. Non-Newtonian Fluid Mech.*, **8**, 261 (1981).
28. N. Y. Tuna and B. A. Finlayson, 'Exit pressure calculations from numerical extrudate swell results', *J. Rheol.*, **28**, 79 (1984).
29. R. D. Wesson and T. C. Papanastasiou, 'Flow singularity and slip velocity in plane extrudate swell computations', *J. Non-Newtonian Fluid Mech.*, **26**, 277 (1988).
30. N. Phan-Thien, 'Influence of wall slip on extrudate swell: a boundary element investigation', *J. Non-Newtonian Fluid Mech.*, **26**, 327 (1988).
31. J. M. Marchal and M. J. Crochet, 'A new mixed finite element for calculating viscoelastic flow', *J. Non-Newtonian Fluid Mech.*, **26**, 77 (1987).
32. F. Horsfall, 'A theoretical treatment of die swell in a Newtonain liquid', *Polymer*, **14**, 262 (1973).
33. A. Dutta and M. E. Ryan, 'Dynamics of a creeping Newtonian jet with gravity and surface tension: a finite difference technique for solving steady free-surface flows using orthogonal curvilinear coordinates', *AIChE J.*, **28**, 220 (1982).
34. A. Settari and K. Aziz, 'A generalization of the additive correction methods for the iterative solution of matrix equations', *SIAM J. Numer. Anal.*, **10**, 506 (1973).
35. S. V. Patankar, 'A calculation procedure for two-dimensional elliptic situations', *Numer. Heat Transfer*, **4**, 409 (1981).
36. M. Gottlieb, and R. B. Bird, 'Exit effects in non-Newtonian liquids. An experimental study', *Ind. Eng. Chem. Fund.*, **18**, 357 (1979).
37. B. A. Whipple and C. T. Hill, 'Velocity distributions in die swell', *AIChE J.*, **24**, 664 (1978).
38. K. Higashitani, H. Nishio and I. Hara, 'Velocity profile variation of a viscoelastic fluid around a die exit', *Proc. 7th Int. Congr. on Rheology*, Gothenburg, 1976, p. 478.
39. J. S. Vrentas, C. M. Vrentas and A. F. Shirazi, 'Downstream boundary conditions for vertical jets', *AIChE J.*, **31**, 1044 (1985).
40. C. J. Coleman, 'A note on the stick-slip and die-swell problems for a second order fluid', *J. Non-Newtonian Fluid Mech.*, **3**, 288 (1977/1978).
41. J. S. Vrentas and J. L. Duda, 'Effect of axial diffusion of vorticity on flow development in circular conduits: Part II. Analytical solution for low Reynolds numbers', *AIChE J.*, **13**, 97 (1967).
42. D. H. Michael, 'The separation of a viscous liquid at a straight edge', *Mathematika*, **5**, 82 (1958).
43. H. K. Moffatt, 'Viscous and resistive eddies near a sharp corner', *J. Fluid Mech.*, **18**, 1 (1964).
44. P.-W. Chang, T. W. Patten and B. A. Finlayson, 'Collocation and Galerkin finite-element methods for viscoelastic fluid flow—I', *Comput. Fluids*, **7**, 267 (1979).
45. A. Dutta, 'A theoretical analysis and experimental study of extrusion blow molding', *Ph.D. Thesis*, State University of New York at Buffalo, Buffalo, New York, 1981.
46. D. V. Boger, R. Gupta and R. I. Tanner, 'The end correction for power-law fluids in the capillary rheometer', *J. Non-Newtonian Fluid Mech.*, **4**, 239 (1978).
47. C. J. Coleman, 'A finite element routine for analysing non-Newtonian flows, Part I: Basic method and preliminary results', *J. Non-Newtonian Fluid Mech.*, **7**, 289 (1980).
48. M. A. McClelland and B. A. Finlayson, 'Heat transfer effects in extrudate swell of elastic liquids', *J. Non-Newtonian Fluid Mech.*, **27**, 363 (1988).
49. K. Adachi and N. Yoshioka, 'Tube exit flows and laminar Newtonian jets in the atmosphere', *Proc. IX Int. Congr. on Rheology*, Mexico, 1984, p. 329, Universidad Nacional Autonoma de Mexico, Mexico (1984).
50. R.-J. Fischer, M. M. Denn and R. I. Tanner, 'Initial profile development in melt spinning', *Ind. Eng. Chem. Fund.*, **19**, 195 (1980).
51. K. Adachi, 'Laminar jets of a plane liquid sheet falling vertically in the atmosphere', *J. Non-Newtonian Fluid Mech.*, **24**, 1 (1987).